Effect of viscous-convective subrange on passive scalar statistics at high Reynolds number

Kedar Prashant Shete, David J. Boucher, James J. Riley, and Stephen M. de Bruyn Kops

Phys. Rev. Fluids **7**, 024601 — Published 22 February 2022

DOI: 10.1103/PhysRevFluids.7.024601

Effect of viscous-convective subrange on passive scalar statistics at high Reynolds number

Kedar Prashant Shete,* David J. Boucher, and Stephen M. de Bruyn Kops
Department of Mechanical and Industrial Engineering,
University of Massachusetts Amherst, Amherst, Massachusetts, USA

James J. Riley
Department of Mechanical Engineering, University of Washington, Seattle, Washington, USA

An assumption common to many approaches to understanding and modeling turbulent mixing is that the statistics of a passive scalar at small length scales will approach the analogous statistics of the velocity field as the scale separation increases between the flow-specific outer scales and the small scales of interest. This assumption follows from the hypotheses of Kolmogorov, Oboukhov, Corrsin, and Batchelor, although it is well recognized that differences in the scalar and velocity dynamics prevent the overall statistics of the two being the same. Considerable research on the effect of Reynolds number and Schmidt number on the scalar statistics has shown that the assumption is not very good at either high Reynolds number or high Schmidt number individually. Because of limitations in laboratory measurements, direct numerical simulations (DNSs), and in-situ measurements of the ocean and atmosphere, it is difficult to obtain data in which the Reynolds number is high enough for an unequivocal inertial-convective subrange, and the Schmidt number is simultaneously high enough for a clear viscous-convective subrange. Our hypothesis is that, when both subranges exist, then there is sufficient scale separation in the velocity field for its statistics to be approximately universal, and also sufficient additional scale separation for the scalar to relax so that its small-scale statistics approach those of the velocity. We explore this hypothesis with DNS resolved on up to $14256 \times 14256 \times 14256$ grid points, Taylor Reynolds number $\mathrm{Re}_\lambda = 633$, and Schmidt number $\mathrm{Sc} = [0.1, 0.7, 1.0, 7.0]$, with the aim of studying the validity of this hypothesis for mixing in air and water. When the Schmidt number is not greater than unity at high Reynolds number, a viscous-convective subrange does not exist and we find that small-scale isotropy, the intermittency exponent, and the probability density function (PDF) of the scalar dissipation rate are all much different from the analogous velocity statistics, as reported widely in literature. However, when the Schmidt number is greater than unity at high Reynolds number, inertial-convective and viscous-convective subranges both exist, and the velocity and scalar statistics are similar. Since this similarity is a consequence of the presence of both inertial convective and viscous convective subranges, it is achieved only at both high Reynolds and Schmidt numbers, and the statistics show a sharp change when the Schmidt number is changed from from 1 to 7. This suggests that at high Reynolds numbers, the modelling assumption of similarity between velocity and scalar statistics is valid for mixing in water, but not in air.

I. INTRODUCTION

A passive scalar is stirred by fluid turbulence without affecting the velocity dynamics. So it is tempting to base models for scalar transport on those for momentum transport. Indeed, the hypotheses of Oboukhov [1], Corrsin [2] and Batchelor [3, 4] for scalars are very similar to those of Kolmogorov [5] and Oboukhov [6, 7] for velocity. Given that the transport equations for passive scalars and momentum have different mathematical forms, for this and other reasons [8] we should not expect the transport of momentum and passive scalars to be completely analogous. Nevertheless, considerable attention is paid to the differences between velocity and scalar statistics in the literature reviewed in, e.g., [9, 10]. In this paper we consider three scalar statistics and the analogous velocity statistics: (1) the skewness of the scalar gradient; (2) the internal intermittency exponent for the scalar; and (3) the probability density function of the dissipation rate of scalar variance. We study them in the context of direct numerical simulations (DNSs) of homogeneous isotropic turbulence for four scalars with Schmidt numbers Sc = 0.1, 0.7, 1.0, and 7.0; each field is transported by the same velocity field, with Taylor Reynolds number $\mathrm{Re}_\lambda = 633$, which is high enough that there is a inertial subrange and, for Sc=7, a clear viscous-convective subrange.

We defer a review of the literature on each of these statistics until §IV so that we can discuss our results in the context of the literature. Before that, in §II, we provide some background and notation regarding turbulence

* kshete@umass.edu

subranges relevant to passive scalars, and a summary of the scalar spectrum model proposed by Hill [11], which we use to aid in interpreting our data from DNS. Following that, in §III, is an overview of our simulation data base along with statistics showing the existence of inertial-convective and viscous-convective ranges. Then in §IV we discuss the aforementioned scalar statistics. Some conclusions are drawn in §V.

II. BACKGROUND

If the Reynolds number of a flow is not sufficiently high then it is broadly understood that the dynamics are dominated by the large scales in length and time, which are flow specific and are unlikely to be the same for the velocity and scalar. Therefore, the concepts that scalar statistics can have a universal form and might be related to velocity statistics inherently include the assumption of high Reynolds number. Indeed, high Reynolds number is the starting point for the classical hypotheses of Kolmogorov, Oboukhov, Corrsin, and Batchelor (KOCB) [1, 2, 5–7]. Here we review these hypotheses and propose an additional requirement of the existence of both inertial-convective and viscous-convective subranges. We then consider whether they can be sufficiently satisfied by presenting state-of-the-art direct numerical simulations (DNSs) that fulfil our hypothesized requirement, which also form the basis for our analyses of scalar statistics later in this paper.

A. Brief review of the classical hypotheses

Let us define D to be the molecular diffusivity of the scalar and ν to be the kinematic viscosity so that the Schmidt number is $\mathrm{Sc} \equiv \nu/D$. It is assumed that the flow is homogeneous and isotropic and that ϵ is the average dissipation rate of turbulence kinetic energy, in contrast to the local instantaneous values ϵ_0. With these definitions, dimensional reasoning leads to the Kolmogorov, Batchelor, and Corrsin length scales defined, respectively, as

$$\eta_k = \left(\frac{\nu^3}{\epsilon}\right)^{1/4}, \quad \eta_b = \left(\frac{\nu D^2}{\epsilon}\right)^{1/4}, \quad \eta_c = \left(\frac{D^3}{\epsilon}\right)^{1/4}, \tag{1}$$

with the corresponding Kolmogorov and Corrsin times scales

$$\tau_k = \left(\frac{\nu}{\epsilon}\right)^{1/2}, \quad \tau_c = \left(\frac{D}{\epsilon}\right)^{1/2}. \tag{2}$$

Only two of the three length scales in (1) can be independent and there is a question of which, if any, are relevant in a given flow. Batchelor [3] reasons that η_b is not relevant if $Sc < 1$ and η_c is not relevant if $Sc > 1$. More generally, Kolmogorov's first hypothesis leads us to conclude that none of the length and time scales in (1) and (2) can be expected to be relevant unless there exist small scale motions that are isotropic with universal form uniquely determined by ϵ and ν.

With the foregoing hypothesis of an isotropic and universal equilibrium subrange at small scales, it follows that an inertial subrange can exist for length scale ℓ between some large scale L characteristic of the energetic motions and η_k provided $L \gg \ell \gg \eta_k$; this is Kolmogorov's second hypothesis [5]. The analagous hypothesis for the scalar is that an inertial-convective subrange can exist for $L \gg \ell \gg \eta_c$ [1, 2]. In the case of $Sc > 1$, a viscous-convective subrange is also hypothesized to exist [3].

The inertial, inertial-convective, and viscous-convective subranges, respectively, can be expressed in terms of dimensionless spectra as

$$\begin{aligned} f(\kappa\eta_k) &= E(\kappa)\kappa^{5/3}/\epsilon^{2/3}\ , \\ g(\kappa\eta_k) &= E_\phi(\kappa)\kappa^{5/3}\epsilon^{1/3}/\chi \\ h(\kappa\eta_k) &= E_\phi(\kappa)\kappa\epsilon^{1/2}/(\chi\nu^{1/2})\ . \end{aligned} \tag{3}$$

Here κ is the magnitude of the wave number vector, $E(\kappa)$ and $E_\phi(\kappa)$ are the shell-averaged kinetic energy and scalar variance spectra, and χ is the molecular dissipation rate of scalar variance. If Kolmogorov's second hypothesis holds along with the analagous hypotheses of Oboukhov, Corssin, and Batchelor, then $f(\kappa\eta_k)$, $g(\kappa\eta_k)$, and $h(\kappa\eta_k)$ will take on universal values for, respectively, the Kolmogorov constant C_k , the Corrsin-Oboukhov constant C_{oc} , and the Batchelor constant C_b .

The spectral forms from (3) are plotted in cartoon form as figure 1. We have used "textbook" values for C_k , C_{oc} ,

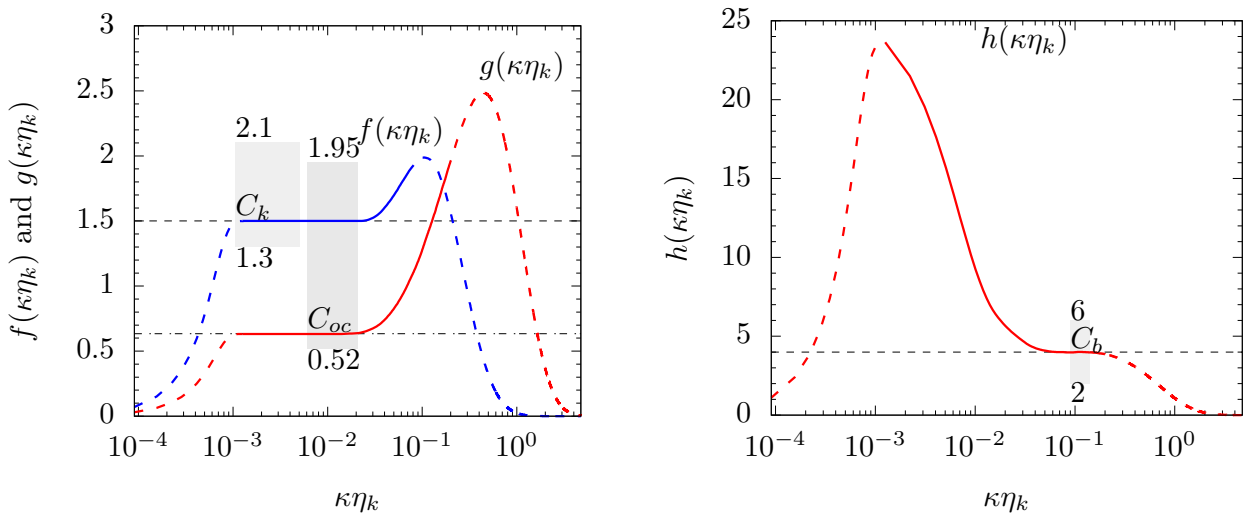

FIG. 1. Sketches of scaled spectra. Solid portions of the curves are the inertial, inertial-convective, and viscous-convective spectral subranges defined by (3) with commonly used values for C_k , C_{oc} , and C_b . The gray shadings indicate non-exhaustive ranges of these constants collected from the literature and tabulated in Table I.

Source	**Flow**	C_k	C_{oc}	C_b
Paquin and Pond [12]	Temperature and humidity fluctuations over the ocean	1.3	1.37 ± 0.2	
Gibson and Schwarz [13]	Flow of saline/heated water in test section	1.34 ± 0.06	0.58 ± 0.08	4
Grant et al. [14]	Temperature and velocity fluctuations in the ocean	-	0.52 ± 0.1	3.9 ± 1.5
Lin and Lin [15]	Temperature fluctuations in subsonic open circuit wind tunnel	-	1 ± 0.1	-
Williams and Paulson [16]	Temperature and velocity fluctuations in atmospheric boundary layer	1.65 ± 0.03	1.67	4 to 6
Champagne et al. [17]	Temperature, velocity and humidity fluctuations in atmospheric boundary layer	1.53 ± 0.06	0.75 ± 0.03	-
Boston and Burling [18]	Velocity and temperature fluctuations over tidal mud flat	1.53 ± 0.06	1.35 ± 0.04	-
Gibson et al. [19]	Velocity and temperature measurements above the ocean	2.1	1.95	-
Clay [20]	Temperature spectra in air, water and mercury	-	0.92 ± 0.08 0.94 ± 0.03 0.87 ± 0.22	-
Qian [21, 22, 23]	Theoretical; non-equilibrium statistical mechanics with a perturbation-variation approach	1.2	0.61	$2\sqrt{5}$
Watanabe and Gotoh [24]	DNS at $\mathrm{Re}_\lambda = 427$ and $Sc = 1$	1.61 ± 0.09	0.68 ± 0.04	-
Antonia and Orlandi [25]	DNS at $\mathrm{Re}_\lambda = 850$ and $Sc = 0.7$ to $Sc = 15$	-	-	3

TABLE I. Values of C_k , C_{oc} and C_b reported through experimental results. A few numerical and theoretical values are also listed.

and C_b while acknowledging a wide range of values is reported for each in the literature; we capture the range for each constant with gray bars on the figure and tabulated the literature values in Table I.

Lastly in this section, we observe that η_b, η_c, and τ_c depend on ϵ but not on χ. In words, the diffusive length and time scales of the scalar are assumed to depend on the dissipation rate of kinetic energy and not the dissipation rate of scalar variance. This assumption, which goes back at least as far Oboukhov [1], is part of the background material in modern reviews and textbooks [e.g. 26, 27]. We note the widespread use of this assumption to support the idea that we return to several times in this paper, namely that there is some expectation that small-scale scalar statistics can be expected to follow those of velocity in high Reynolds number flows.

B. Hill's model

In the classical hypotheses of KOCB, the dissipation rate of kinetic energy is taken to be zero in the inertial subrange and the dissipation rate of scalar variance zero in the inertial-convective and viscous-convective subranges. The dissipation occurs in the dissipation subrange. Inherent in the definitions of the length and time scales given in (1) and (2) are the assumptions that eddies in the dissipation range are in equilibrium with the larger eddies in the flow and that the statistics of the small eddies are universal. Significant research has been done to model the spectral form in the dissipation subranges of the velocity and scalar [e.g. 11, 28].

Several efforts have been made to produce a model that spans multiple subranges. One such is Pope's model spectrum for velocity [29, equation 6.246]. Meyers and Meneveau [30] propose a model for the velocity spectra that accounts for the the so-called "bottleneck" effect observed in velocity spectra between the inertial and dissipation subranges. Much earlier, though, Hill [11] proposed a set of four model spectra for a passive scalar that are based on assumptions about the spectral transfer function without any assumption about the energy spectrum itself. Because assumptions are made about the transfer function rather than the spectrum, the models take the form of differential equations that are solved numerically to yield the model spectra. Thus, with the assumptions of Oboukhov, Corrsin, and Batchelor for the inertial-convective subrange, plus an assumption for the transfer function in the dissipation range, the transition between the two emerges rather than being prescribed.

The difference between Hill's four models is in the assumptions about the dissipation subrange. His own comparisons with data available at the time of the paper suggest that the fourth model in the set is very promising, and Muschinski and de Bruyn Kops [31] showed excellent agreement for passive scalar mixing in homogeneous isostropic turbulence (HIT) with $\mathrm{Re}_\lambda = 400$, and $\mathrm{Sc} = 0.7$ and 1. The model spectrum is the solution to

$$\frac{d}{d\xi}\left\{\xi^{14/3}(\xi^{2b}+1)^{-1/3b}\frac{d}{d\xi}\left[\xi^{-2}E_\phi(\xi\kappa^\dagger)\right]\right\} = \frac{22}{3}\frac{C_{oc}}{\mathrm{Sc}}(\kappa^\dagger\eta_k)^{4/3}\xi^2 E_\phi(\xi\kappa^\dagger)\ , \tag{4}$$

where $\xi = \kappa/\kappa^\dagger$ and $\kappa^\dagger$ satisfies $a = \kappa^\dagger\eta_k$ for some value of a that Hill hypothesized to be a universal constant. If a value of C_{oc} is assumed from the literature, e.g,, as in Table I, then the two model parameters a and b remain to be determined, as considered further in §III C

C. Internal intermittency

KOBC assume that ϵ and χ are uniform in space for homogeneous and isotropic turbulence. It was, however, recognized [32] at the time Kolmogorov's first and second hypotheses [5] were published that ϵ is not constant in space even in HIT flow. Instead, Kolmogorov and Oboukhov [32, 33] noted that turbulence is intermittent at the small scales and ϵ should be interpreted as the expected value of the local dissipation rate ϵ_0. Similar reasoning applies to the relationship between χ and its local value χ_0. Generalizing on this refined hypothesis about ϵ, Novikov and Stewart [34] postulated that if ϵ_0 is averaged over a volume with characteristic length scale r to form ϵ_r then

$$\left\langle \epsilon_r^2 \right\rangle \sim r^{-\mu}\ , \tag{5}$$

where $\langle\cdot\rangle$ denotes an ensemble average so that the lefthand side of (5) is the variance of ϵ_r. The analogous expression for the variance of χ_0 is

$$\left\langle \chi_r^2 \right\rangle \sim r^{-\mu_\phi}\ . \tag{6}$$

In some applications, intermittency is very important. For example, the high rates of strain associated with high values of χ_0 can extinguish combustion even if χ is sufficiently low to allow combustion. High values of ϵ_0 are associated with damage to machinery operating in flows with high Reynolds number. In general, intermittency is expected to increase with increasing Reynolds number [e.g. 35–37]. Ishihara et al. [38] use DNS to consider the relationship between μ and $E(\kappa)$ in the inertial range.

D. Direct numerical simulation

Direct numerical simulation (DNS) typically refers to the solution of the equations of motion for a flow without using turbulence models. Since its inception in 1972 [39], it has become an important research tool, particularly for considering flows with very simple initial and boundary conditions. Examples include its application to stratified turbulence [40], channel flow [41], mixing layers [42], decaying homogeneous isotropic turbulence [43], and self-similar

scalar mixing layers [44]. An advantage of DNS over other research tools is that it provides flow data as a function of three spatial dimensions and time.

The first criterion for a DNS to be useful for understanding flow physics is that the DNS technique yields a numerically accurate solution to the governing equations. All of the examples of DNS cited in the preceding paragraph, as well as our DNS reported in §III, used some form of spectral method, and spectral methods, for a given resolution, have very fast convergence and very small phase errors when compared to other methods [45]. So the focus in the literature is typically on truncation error, or small-scale resolution. One of the earlier thumbrules for adequate resolution is that, for the scalar variance to decay at a rate independent of small-scale resolution in HIT, the grid spacing must be no more than approximately three times the Kolmogorov length scale [46]. Since then it has been observed that sufficient resolution is not an absolute standard but rather is dependent on the quantities of interest. For example, a simulation with sufficient resolution to accurately compute the expected value of turbulent fluctuations may not have the resolution required to compute accurately the probability density function (PDF) of those fluctuations. Increasing the resolution results in intermittency effects at small scales, which in turn demands higher resolution to resolve the PDF at small scales.

Yeung et al. [47] provide recent analyses of spatial and temporal resolution in the context of very large HIT DNS comparable to those reported in §III. Using the PDFs of ϵ_0 and local enstrophy as figures of merit, they conclude that the grid spacing must be approximately η_k or smaller for the PDFs to converge for $\mathrm{Re}_\lambda \approx 650$. They also give the Courant number requirements in terms of the time-stepping algorithm they used. Shete and de Bruyn Kops [48] arrive at comparable space and time resolution requirements with a completely different approach, namely by determining the resolution required for the area of an isosurface, computed from an exact expression via Monte-Carlo integration, to converge. As shown in §III, the simulations reported in this paper meet the resolution requirements determined by Yeung et al. [47] and Shete and de Bruyn Kops [48]. However, using even finer resolution for the scalar ϕ_a would be interesting as a future study.

A second criterion for a DNS to be useful is that the simulated flow be appropriate for the research being conducted. For example, obviously a flow at moderate Reynolds number is of limited use in understanding turbulence at high Reynolds number. The challenge with the foregoing statement is in the definition of "high Reynolds number." Our rationale is that our simulations should demonstrate broad agreement with KOBC scaling before being applied to studying scalar statistics at high Reynolds number. Simulations of finite size cannot be perfectly isotropic, and simulations that can be run on existing computers do not have the scale separation for the inertial and inertial-convective subranges to be completely free of molecular effects as hypothesized by KOBC. Nevertheless, small-scale isotropy can be closely approximated and the scaling ranges described by (3) can be observed with values of C_k , C_{oc} , and C_b similar to those in Table I.

A significant limitation of DNS is in the temporal and spatial resolution of the large-scale structures. While laboratory measurements can typically be made over long periods of time to accumulate excellent statistics of the large scales in length and time, it is not practical to run DNS at high Reynolds number in very large domains (relative to the integral length scale of the simulated flow) or for very long times. de Bruyn Kops and Riley [43] show that the domain size for homogeneous isotropic turbulence must be approximately 20 integral length scales if the simulation is to exhibit the energy decay rates predicted by theory and observed in laboratory experiments [49]. This large-scale resolution requirement, coupled with the small-scale resolution requirements reviewed above, precludes high Reynolds number simulations on existing computers. This is why the largest simulations to date have very limited large-scale resolution and employ synthetic forcing of the large scales to maintain the flows statistically stationary [47, 48]. It is well recognized that the dissipation rate is slightly lower in a forced simulation than in the analogous decaying simulation of HIT, as first reported by Sreenivasan [50].

III. SIMULATION DATABASE

The simulated flows used for this research are a subset of those reported by Shete and de Bruyn Kops [48]. Specifically we consider the velocity field denoted R633 with $\mathrm{Sc} = [0.1, 0.7, 1.0, 7.0]$. The nomenclature R633 refers the value of the Taylor Reynolds number $\mathrm{Re}_\lambda = u'\lambda/\nu$ with u' the r.m.s. velocity and λ the Taylor microscale.

The simulations solve the equations

$$\nabla \cdot \vec{u} = 0 \tag{7a}$$

$$\frac{\partial \vec{u}}{\partial t} + \vec{u} \cdot \nabla \vec{u} = -\nabla p + \nu \nabla^2 \vec{u} + \vec{b} \tag{7b}$$

$$\frac{\partial \phi}{\partial t} + \vec{u} \cdot \nabla \phi = -\vec{u} \cdot \nabla \Phi + D \nabla^2 \phi \ , \tag{7c}$$

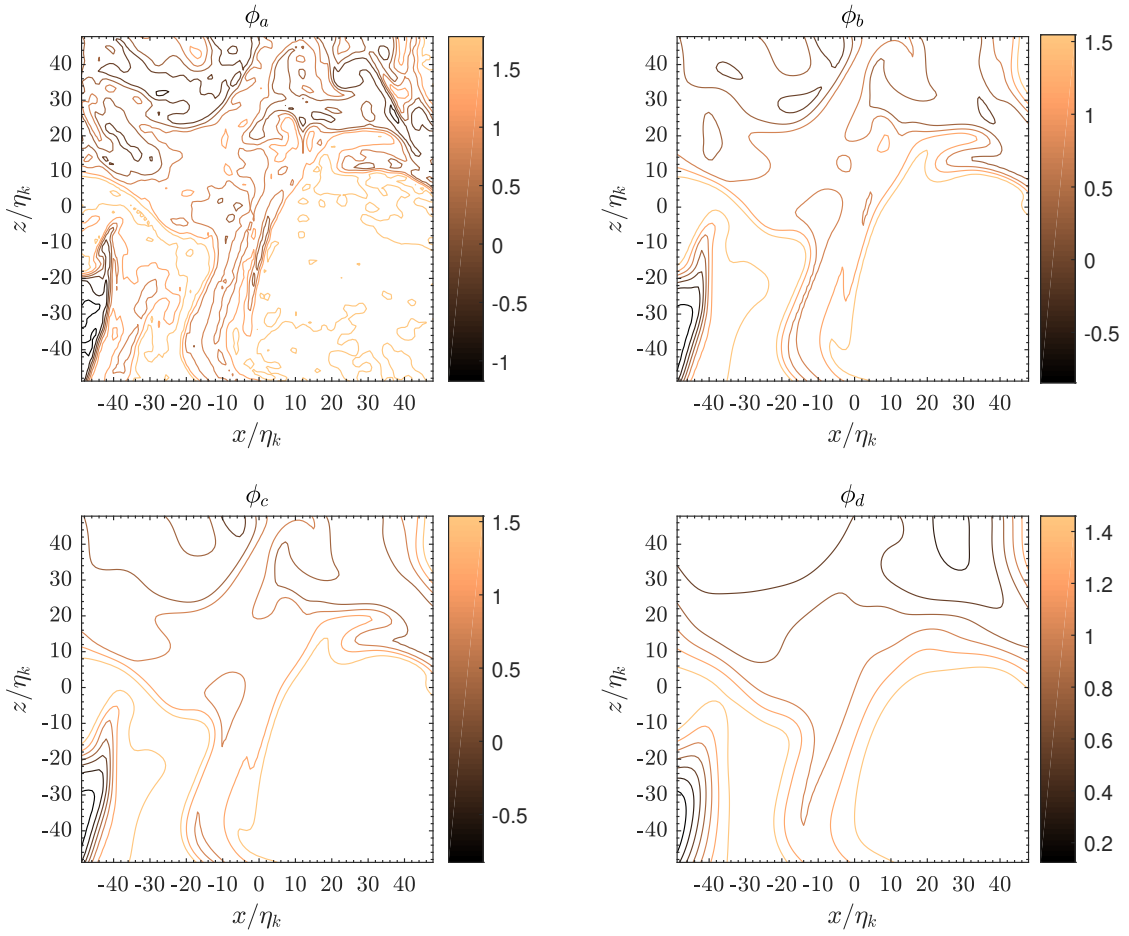

FIG. 2. Scalar contours for each simulation case on a region of the xz-plane centered at $y = 0$; the region is approximately 1/50th of the size of the full plane in each direction. The scalar values are normalized by the RMS value for the region shown, and there are eight contours spaced evenly between the minimum and maximum values. The data plotted are at a lower resolution than the actual simulations and are intended purely for visualization.

in a periodic domain with coordinate system $\vec{x} = [x, y, z]$ and corresponding velocity vector $\vec{u} = [u, v, w]$. The pressure p has been divided through by the (constant) density and $\vec{b}$ is a time-varying force applied to maintain the large length scales of the flow to be statistically stationary. The passive scalar is decomposed into $\Phi + \phi$, with time-invariant Φ having a uniform gradient in the direction of w, and being uniform in the other spatial directions; ϕ denotes the fluctuations relative to Φ. The equations are solved with Fourier-spectral discretization in space, a fractional step method third-order accurate in time, and full dealiasing by truncation in Fourier space.

The velocity fields are forced in Fourier space to have a target shell-averaged kinetic energy spectrum given by Pope's model spectrum with his $p_0 = 2$ and his $c_L = 6.78$ [29, (equation 6.247)]. A second-order ordinary differential equation is advanced in time for each of the shells of the shell-averaged spectrum having wave number magnitude less than six times the smallest non-zero wavenumber; this determines of the amount of energy to add to that shell during a time step. The energy is distributed randomly across all wave numbers in the shell subject to the constraint of continuity. The solution to these differential equations and the random distributions produces the Fourier-space equivalent of $\vec{b}$. This approach is introduced by Overholt and Pope [51] to efficiently converge a simulation to a target spectrum; Rao and de Bruyn Kops [52] review a variety of forcing techniques for the type of simulation used for this research. After a simulation is determined to be statistically stationary based on mean quantities, it is advanced for an additional large eddy turnover time before taking a snapshot for analysis. Contour plots for each simulation are in figure 2.

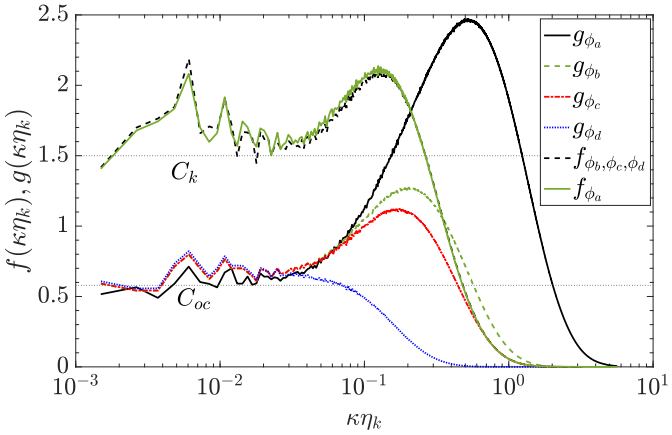

FIG. 3. Scaled velocity and scalar spectra $f(\kappa\eta_k)$ and $g(\kappa\eta_k)$ for our data.

$\mathrm{Re_L}$		12150		
Re_λ		633		
$\mathcal{L}/L$		5.56		
$\kappa_{max}\eta_k$		5.65		
N		14256		
Scalar	ϕ_a	ϕ_b	ϕ_c	ϕ_d
Sc	7	1	0.7	0.1
Pe_λ	4428.57	632.65	442.86	63.27
$\eta_k/\Delta x$	2.70	1.55	1.55	1.55
$\eta_c/\Delta x$	0.63	1.55	2.02	8.71
$\eta_b/\Delta x$	1.02	1.55	1.85	4.90
$\tau_k/\Delta t$	1202.44	779.68	779.68	779.68
$\tau_c/\Delta t$	454.48	779.68	931.89	2465.55

TABLE II. Velocity and scalar parameters and statistics for the simulations. N and $\kappa_{max}\eta_k$ are shown for the highest resolution ($\mathrm{Sc} = 7$) which corresponds to ϕ_a, lower resolution is used for the cases with ϕ_b, ϕ_c and ϕ_d which are at lower Sc number.

A. Spatial and temporal resolution

The simulation data base includes four scalar fields ϕ_a, ϕ_b, ϕ_c, and ϕ_d. All four were advanced in time with the same velocity field until statistical stationarity was observed, and then for an additional large-eddy turnover time, with resolution $8190 \times 8190 \times 8190$ grid points. The resolution of the velocity field and of the scalar ϕ_a ($\mathrm{Sc} = 7$) was then increased to $14256 \times 14256 \times 14256$ grid points and advanced in time until the scalar statistics had converged.

Domain-averaged statistics are tabulated in Table II. $\mathcal{L}$ is the simulation domain size, L is the integral length scale, κ_{max} is the highest wave number magnitude after dealiasing, N is the number of grid points in each direction, Δx is the grid spacing, Δt is the time step for the third-order Adams Bashforth time stepping algorithm, and $\mathrm{Pe}_\lambda = \mathrm{Re}_\lambda \mathrm{Sc}$ is the Taylor Péclet number. Velocity statistics are included only for the high-resolution field because, since the simulations are forced to be statistically stationary, the domain-averaged statistics differ very little between the two velocity fields. The small-scale spatial resolution and temporal resolution meet the criteria discussed in §II D.

B. Consistency with similarity hypotheses

There are two principle assumptions in the classical hypotheses of KOBC, the first being isotropy and the second being sufficient separation between the energy-containing length scales and the length scales associated with dissipation. The local isotropy of velocity fields generated by the same method we use here is well documented [e.g. 53] and so we limit our discussion of isotropy to that of the skewness of the scalar derivatives, which is the topic of §IV A. In §II, scale separation is summarized in terms of (3) and we propose that, if these spectral forms are evident in DNS data, then the DNS may be expected to be informative about small-scale statistics at high Reynolds number.

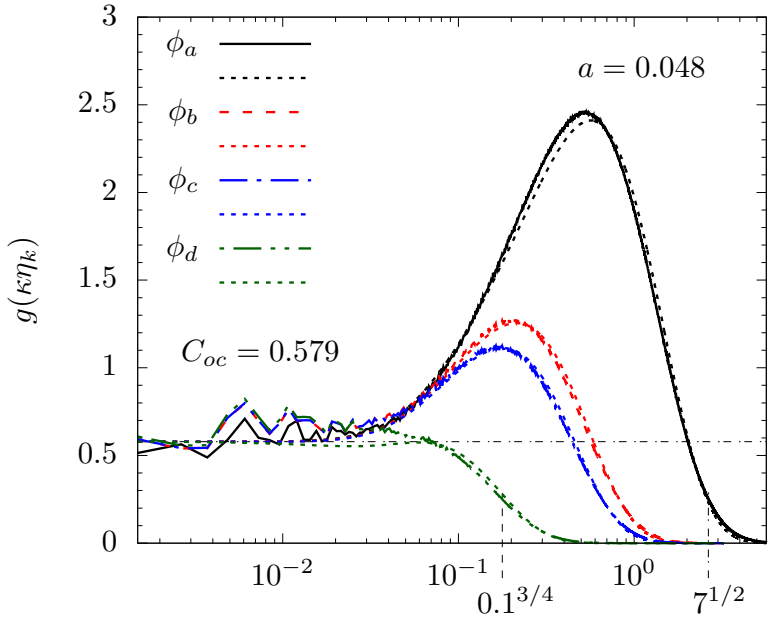

FIG. 4. Solid and pattern curves are $g(\kappa\eta_k)$ for ϕ_a, ϕ_b, ϕ_c and ϕ_d. The small-dashed curves in same color are Hill's model fit to the DNS data as discussed §III C. The horizontal dash-dot line is is the value for C_{oc} for the dashed lines. The location of $\kappa\eta_c$ for case ϕ_d and $\kappa\eta_b$ for case ϕ_a are indicated on the horizontal axis to indicate graphically the resolution of the simulations.

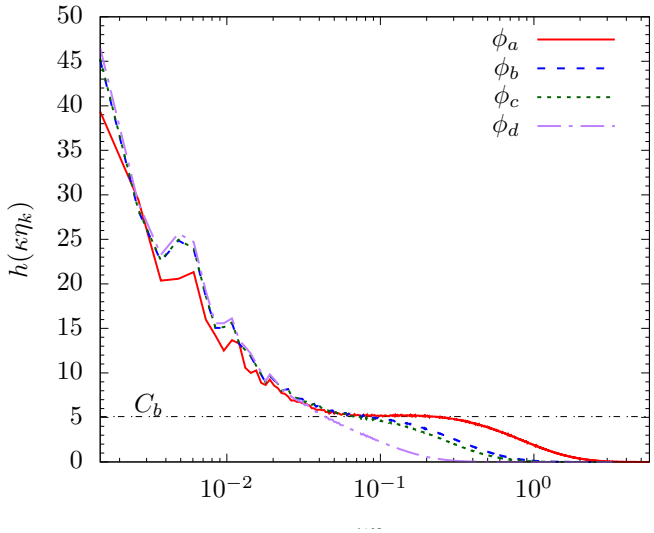

FIG. 5. Scaled scalar spectrum $h(\kappa\eta_k)$.

The DNS spectra are plotted in Figs. 4 and 5. The axes are scaled so that the hypothesized spectra (5) will plot as horizontal plateaus with the values of C_{oc} and C_b shown on the plots. It can be inferred from Fig. 4 that an inertial-convective range exists with $C_{oc} \approx 0.579$. This value of C_{oc} is toward the low end of those tabulated in Table I, and we recall from §II that ϵ in forced simulations has been observed to be smaller than that in decaying simulations, which is consistent with lower C_{oc} . The velocity spectrum, plotted in Shete and de Bruyn Kops [48], indicates a value of C_k slightly higher than the textbook value of 1.5, which is again consistent with ϵ being slightly lower in forced HIT than in other flows; we do not duplicate this plot here. The scalar spectrum for case ϕ_a is plotted with the incorrect value of C_{oc} in Shete and de Bruyn Kops [48] due to an error in χ.

The spectrum in Fig. 5 is scaled so that the viscous-convective subrange, if it exists, will appear as a horizontal plateau with the value C_b . From the figure, a plateau is evident for case ϕ_a with $\mathrm{Sc} = 7$. The value of C_b is toward

the high end of those listed in table I.

C. Use of Hill's model to determine C_{oc}

The Obukhov-Corrsin constant C_{oc} is defined by the plateau in the scaled spectrum $g(\kappa\eta_k)$, but the spectrum in the inertial-convective range tends not to be smooth unless averaging is done in time or a much larger $\mathcal{L}/L$ is used [c.f. 38, 54]. In contrast, the spectrum at higher values of $\kappa\eta_k$ is very smooth because of the large number of smaller eddies in the domain at an instant in time. Because Hill's model spectrum emerges from assumptions about spectral transfer functions rather than assumptions about the spectrum itself, we propose that Hill's model can be used to estimate C_{oc} . To do this, we note that the solution to (4) is very weakly dependent on the constant b and accept Hill's values $b = 1.9$. We then minimize the L1-norm of the difference between the model and DNS spectra by adjusting a and C_{oc} .

The results of fitting Hill's model to the DNS data are plotted in Fig. 4. For each of the four scalar cases, the model agrees very well with the data when $C_{oc} = 0.579$ and $a = 0.048$. We note that the value for C_{oc} is slightly lower than one might estimate by eye.

IV. EFFECT OF SCHMIDT NUMBER

The theme of this paper is to reconsider what Mi et al. [9] refer to as the "classic notion" that the scalar statistics will follow the velocity statistics in HIT. As noted in the introductory paragraph of this paper, there are reasons why they might not.

It has been observed early on by Kraichnan [55] that many characteristics of the scalar field are independent of the velocity field. Nevertheless, if the scalar is passive and there is sufficient scale separation in the velocity field for an approximately universal equilibrium regime to exist, then it is surprising, at least to many researchers, that the small-scale scalar statistics will not be analogous to those of velocity. This argument hinges on their being "sufficient" scale separation, and we conclude in §III that there is sufficient separation for an inertial-convective subrange to be evident and, in the case of ϕ_a, a viscous-convective subrange. We now turn to three very much studied scalar statistics in the context of the current simulations. These statistics are isotropy of the scalar derivatives, internal intermittency, and the PDF of χ.

A. Scalar isotropy

A key assumption in classical similarity theories is that the small scales are statistically isotropic at sufficiently high Reynolds number. This would imply that the odd moments of the scalar derivatives vanish at high enough Reynolds numbers, but nonzero skewness is observed for the scalar derivatives in the direction of the mean gradient even at very high values of Reynolds number [8, 56, 57], which was also reported in the excellent review of Shraiman and Siggia [58]. Since non-zero skewness violates local isotropy, it is apparent that high Reynolds number is not sufficient for the scalar statistics to be isotropic. In fact Sreenivasan [8] notes that local isotropy for passive scalar is not trivially obtained from local isotropy of the velocity. It is possible, though, that high Reynolds number and high Schmidt number together affect isotropy, as we discuss next.

The existence of ramp-cliff structures in the trace of the scalar is well known [10, 58, 59]. Fig. 6 shows typical traces from the current simulations. The ramp-cliff structure is evident in each case. Note that as Sc is increased from one case to the next, the oscillations, e.g., in the cliff structure, also clearly increase. This increase can be understood by examining the nondimensional dissipation rate of ϕ,

$$\chi = \frac{1}{Sc\, Re_L} \left\langle \left(\frac{\partial \phi}{\partial x_i} \right)^2 \right\rangle . \tag{8}$$

It was found by Shete and de Bruyn Kops [48], working with exactly the same DNS data set as used here, that χ was approximately constant, independent of Sc. Therefore,

$$\left\langle \left(\frac{\partial \phi}{\partial x_i} \right)^2 \right\rangle \approx Sc\, Re_L\, \chi_c \,, \tag{9}$$

with χ_c the constant value of χ. Therefore the RMS of ϕ_z should increase linearly with Sc, which is consistent with the increase in oscillations of ϕ with increasing Sc, as seen in the figure. Although the value was χ was found to be

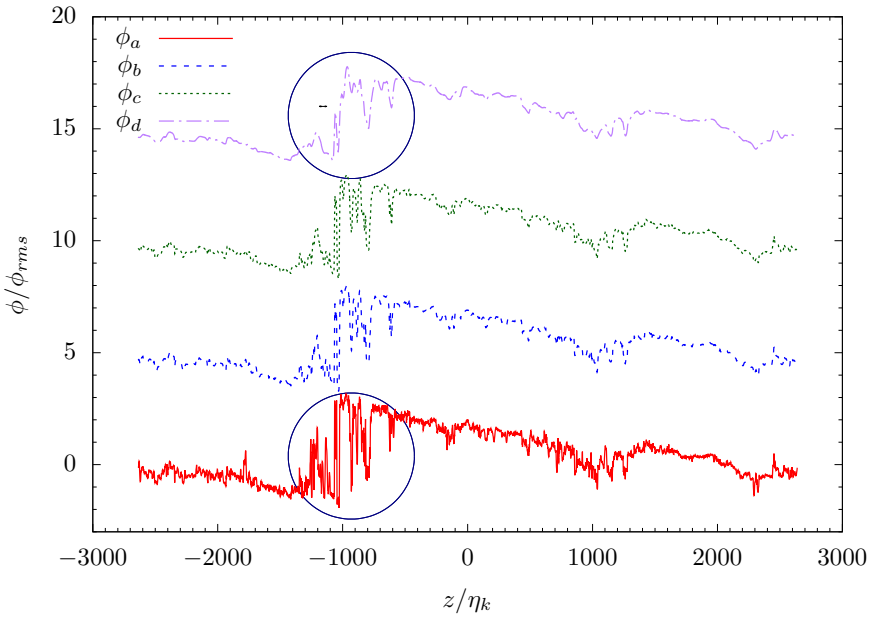

FIG. 6. Trace of scalars in z-direction at $x \approx 0$ and $y = 0$.

approximately unchanging for the data considered here, it should be noted that some of the latest research[60] at $\mathrm{Re}_\lambda = 140$ has found that it could vary at very high Sc, and (8) should be considered an approximation.

To the best of our knowledge, the possible connection between the small scale anisotropy given by the non-zero skewness of scalar derivatives, and the large scale anisotropy given by ramp-cliff structures, is first reported by Mestayer et al. [56]. This is reiterated later by Sreenivasan [8], Shraiman and Siggia [58] and most recently by Sreenivasan [59], who proposes an approximate model for the odd moments of the scalar derivative given as

$$\frac{\langle(\partial\phi/\partial z)^p\rangle}{\langle(\partial\phi/\partial z)^2\rangle^{p/2}} \sim Sc^{-1/2}\mathrm{Re}_\lambda{}^{(p-3)/2}\,. \tag{10}$$

A derivation (motivated by the argument given in Sreenivasan [59]) of this equation is in Appendix A. In this derivation, it is assumed that the Batchelor scale is much smaller than the Kolmogorov scale, which implies that that $Sc = (\eta_b/\eta_k)^{-2}$ is large. Therefore, for large Sc, the skewness of $\partial\phi/\partial z$, S_{ϕ_z}, is expected to behave as $Sc^{-1/2}$ and independent of Re_λ. Fig. 7 contains the values of S_{ϕ_z} which show that our results are consistent with this prediction.

If we assume that $\eta_b \geq \eta_k$, i.e., $\mathrm{Sc} \leq 1$, and $|\ln(\mathrm{Sc})| \leq O(1)$, that η_k is then the scale for the cliff structures, and follow the derivation in Appendix A, the result is that S_{ϕ_z} asymptotes to a constant independent of Sc and Re_λ. This is consistent with the behavior of S_{ϕ_z} for $Sc \leq 1$ in Fig. 7. The transition in behavior of S_{ϕ_z} from constant to $Sc^{1/2}$ is expected to occur close to $Sc = 1$, provided that the assumptions in the derivation are satisfied, i.e., that inertial-convective and viscous-convective subranges are present. Our results are consistent with S_{ϕ_k} asymptoting to a constant at low Sc. They are also consistent with our overarching hypothesis that, when both the inertial-convective and viscous-convective subranges exist, then there is sufficient scale separation in the velocity field for its statistics to be approximately universal, and also sufficient additional scale separation for the scalar to relax so that its small-scale statistics approach those of the velocity.

B. Intermittency Exponents

Having observed that, with an isotropic velocity field, S_{ϕ_z} approaches its isotropic value only when $Sc > 1$, we now consider the effect of Schmidt number on intermittency statistics of the scalar relative to those of velocity. Let us define ϵ_0 and χ_0 to be the local values, in space and in time, of the kinetic energy and scalar variance dissipation rates.

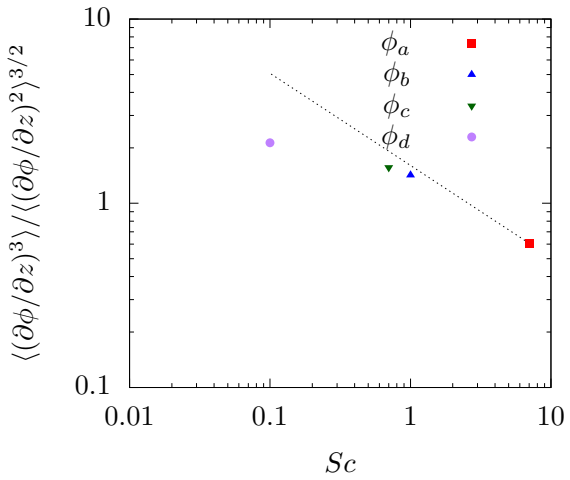

FIG. 7. Skewness of the parallel scalar derivative as a function of the Schmidt number. The dotted line denotes a slope of $Sc^{-1/2}$, as predicted by the model in (10) for high Schmidt number. Our results are consistent with this prediction.

Internal intermittency refers to the fact that both ϵ_0 and χ_0 vary in space and time even for a flow that is statistically stationary and homogeneous. Intermittency can be considered qualitatively in terms of the width of the PDFs of ϵ_0 and χ_0 and we discuss these PDFs in §IV C. First, though, let us narrow our focus to Kolmogorov's hypothesis [32] that if ϵ_0 is averaged over a volume of characteristic length r to form ϵ_r, then its variance $\langle\epsilon_r\rangle$ will vary as a power of r, that is,

$$\langle\epsilon_r\rangle \sim r^{-\mu}\,, \tag{11}$$

with μ being the intermittency exponent. We note that Kolmogorov included an assumption that the PDF of $\log\epsilon_r$ is Gaussian, but this assumption is not an essential part of his hypothesis that μ is universal in the inertial range [34]. Van Atta [61] made the analogous hypothesis for a passive scalar,

$$\left\langle\chi_r^2\right\rangle \sim r^{-\mu_\phi}\,. \tag{12}$$

One of the many implications of intermittency is that ϵ_0 is a random variable. If $E(\kappa)$ and $E_\phi(\kappa)$ are convolved with the PDF of ϵ_0 in place of ϵ to form expressions analogous to (3) then, by Jensen's inequality [62], the resulting average spectra will slope upward with increasing $\kappa\eta_k$ in the regions that $f(\kappa\eta_k)$ and $g(\kappa\eta_k$ exhibit plateaus. Indeed, Ishihara et al. [38] carefully measured the slopes of the average kinetic energy spectra for HIT at $\mathrm{Re}_\lambda \approx 2300$ and observe that they are flatter than $\kappa^{-5/3}$.

Computing μ requires being able to measure ϵ_r directly rather than inferring it from a surrogate based on one or more velocity derivatives. Other than in DNS, though, ϵ_r cannot be measured directly with existing technology, and the maximum Reynolds number accessible with DNS remains very limited. Values of μ at high Reynolds number are typically based on measurements of a surrogate and isotropy is assumed. Almalkie and de Bruyn Kops [53] show that the surrogates for ϵ_r based on either longitudinal or transverse velocity derivatives are more intermittent that ϵ_r itself, and that μ computed from surrogates can be expected to be higher than the true value of μ. Praskovsky and Oncley [63] review studies reporting μ as low as 0.14 and as high as 0.7; the textbook value for μ with r in the inertial range is $\mu = 0.25 \pm 0.05$ [29, 64].

Mydlarski and Warhaft [65] consider grid turbulence in air for seven values of Re_λ ranging from 100 to 731. They report $\mu_\phi \approx 0.2$ at $\mathrm{Re}_\lambda = 100$ and increasing to $\mu_\phi \approx 0.29$ at $\mathrm{Re}_\lambda = 731$. The corresponding values of μ are 0.04 and 0.14. Muschinski [66] reports $\mu \approx 0.15$ and $\mu_\phi \approx 0.3$ in the stable nocturnal boundary layer. Prasad et al. [67] found $\mu_\phi = 0.38 \pm 0.08$ and $\mu = 0.25 \pm 0.05$ in a water jet with jet Reynolds number approximately 3600, which is close to the transition Reynolds number of the jet. In DNS of HIT at $\mathrm{Re}_\lambda = 400$, $\mu \approx 0.25$ and $\mu_\phi \approx 0.3$ [68].

Let us consider the current data beginning with the estimation of μ using Fig. 8. A well recognized challenge in finding μ is that its definition assumes a broad inertial range over which the value is constant. Even at higher Reynolds numbers than we have in our data set, such a scaling range is not observed [63]. Here we take the Taylor microscale λ to be representative of a value of r in the inertial range and compute μ at $r = \lambda$; λ is marked on the figure by a vertical dashed line. From the figure, $\mu = 0.23$. Mydlarski and Warhaft [65] report that $\mathrm{Re}_\lambda = 731$ is too low for the universal value of μ to be observed, assuming a universal value exists. Nevertheless, our data with

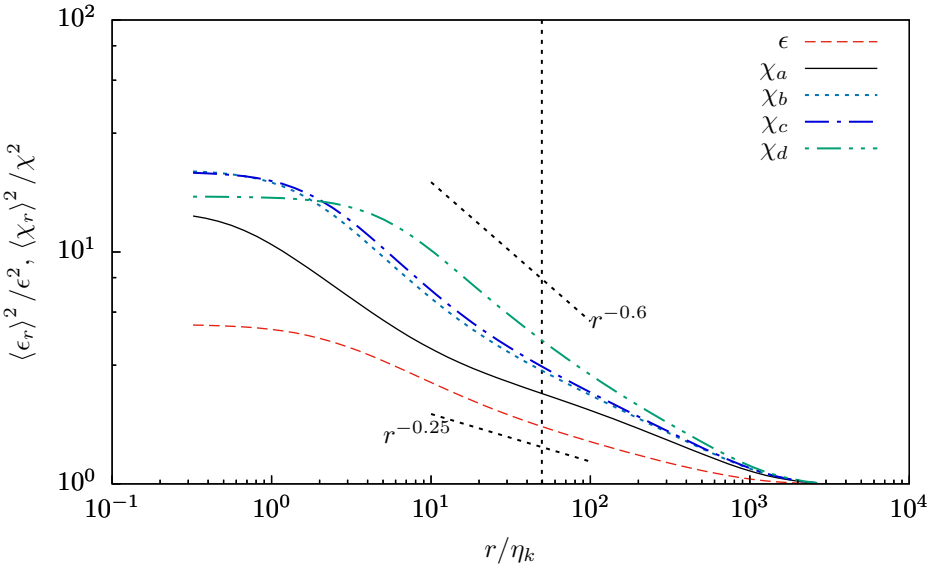

FIG. 8. The scale dependence of the second-order moments of the dissipation rates. The dashed vertical line is drawn at the value of the Taylor microscale. The labels χ_a, etc., are shorthand for χ_r for case indicated by the subscript. ϵ_r and χ_r are averages over spheres of radius r and computed exactly in Fourier space as described by Almalkie and de Bruyn Kops [53].

$\mathrm{Re}_\lambda = 633$ exhibits the textbook value of μ, as does DNS of HIT at $\mathrm{Re}_\lambda = 400$ [68]. We conclude that the current data set has a sufficiently broad inertial range for us to proceed with an analysis of μ_ϕ.

From Fig. 8, the intermittency exponent for the scalar varies monotonically with Sc from $\mu_\phi \approx 0.51$ for case ϕ_d to $\mu_\phi \approx 0.24$ for case ϕ_a. As with μ, these values are measured at $r = \lambda$. If we consider the range $\lambda/2 < r < 2\lambda$ then we find $\mu_\phi = 0.51 \pm 0.1$ for case ϕ_d, and 0.25 ± 0.00 (to two significant figures) for case ϕ_a. Case ϕ_c has the same value of Sc as air, and we observe that the DNS values of $\mu_\phi = 0.38$ and $\mu = 0.23$ are slightly larger than the corresponding values reported by Mydlarski and Warhaft [65] for grid turbulence at $\mathrm{Re}_\lambda = 731$ and Muschinski [66] in the nocturnal boundary layer. For all the cases with $\mathrm{Sc} \leq 1$, the results are consistent with the literature, $\mu < \mu_\phi$. In case ϕ_a with $\mathrm{Sc} = 7$, however, $\mu_\phi \approx \mu$. Therefore, when there exists both inertial-convective and viscous-convective subranges then the intermittency of the scalar is comparable with that of the , at least within the range of Schmidt numbers considered. This is not the result found by Prasad et al. [67] in measurements of a water jet. We observe, though, that the jet Reynolds number in those experiments was not much larger than that for laminar-turbulent transition so that the inertial-convective and viscous-convective subranges were likely very limited. This is consistent with the hypothesis that the Reynolds and Schmidt numbers must both be high for the scalar statistics to be comparable to the analogous velocity statistics.

C. PDFs of dissipation rates

The intermittency exponents are based on the second moments of ϵ_r and χ_r. Higher moments can also be considered to quantify internal intermittency [e.g. 53, 69, 70]. Perhaps a more intuitive, although qualitative, measure of intermittency is the shape of the shape of the PDFs of ϵ_0 and χ_0.

The longitudinal velocity derivative is well known to be negatively skewed, and the PDF of the logarithm of the transverse derivatives are far from Gaussian with left tails that are close to exponential. Yet $P(\log \epsilon_0)$ is close to Gaussian within four or more standard deviations of the mean; here $P(\cdot)$ indicates the PDF of the argument. This is seen in the results of Almalkie and de Bruyn Kops [53, Fig. 6 and 7], who show the PDFs of the velocity derivatives and ϵ_0 for DNS of HIT, of Yeung et al. [47] who discuss the PDF's in the context of numerical resolution, and of Praskovsky and Oncley [63], who show PDFs computed from laboratory data for a range of Reynolds numbers.

While the Gaussian distribution is a good model for $P(\log \epsilon_0)$, except perhaps in the far tails, it has long been recognized that is not a good model for $P(\log \chi_0)$. Antonia and Sreenivasan [71] were apparently the first to report that the righthand tail of the PDF is distinctly inside the standard Gaussian curve. The same characteristic is observed in many simulations and laboratory experiments [e.g. 9, 68, 69] for which phenomenological models have been developed as well[72]. In particular, Vedula et al. [73] report that, although $P(\log \epsilon_0)$ approaches the standard Gaussian with increasing Reynolds number, $P(\log \chi_0)$ shows no such behavior. While the entire PDF is of theoretical

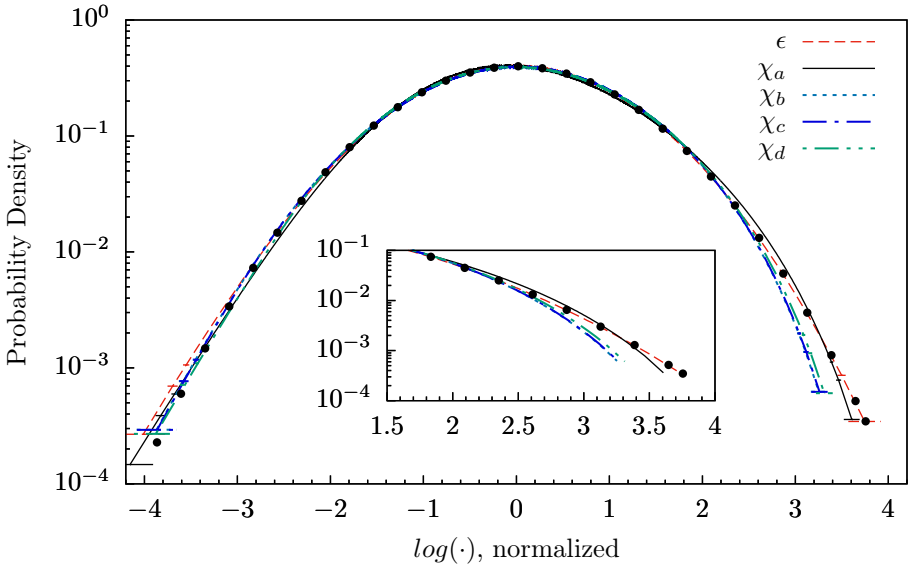

FIG. 9. P.d.f. of the natural logarithm $\log(\chi_0)$ and $\log(\epsilon_0)$ for scalars ϕ_a, ϕ_b, ϕ_c and ϕ_d. Each curve is normalized by its mean and variance per the definition of the standard Gaussian, and the Gaussian is marked with filled circles. The labels χ_a, etc., are shorthand for χ_0 for case indicated by the subscript. The error bars are described in the text and are too short to see except near the tails of the distribution. The curves for χ_b and χ_c are indistinguishable at the resolution of the figure.

interest, the right tail is of practical interest for modeling mixing because, for example, high mixing rate and large χ_0 are synonymous.

Accurately determining $P(\log \chi_0)$ requires that the numerical simulation or laboratory experiment have sufficient spatial resolution to measure χ_0 and also sufficient samples of χ_0. It is also important to take into account the Reynolds number. Shete and de Bruyn Kops [48] show, in DNS of HIT, that the PDFs of the gradient magnitudes are very close to exponential on the righthand side when $\mathrm{Re}_\lambda = 98$, and approximately lognormal when $\mathrm{Re}_\lambda = 633$. For values of Re_λ in between, Sc affects the shape of the PDF. These results suggest that consideration of why the Gaussian distribution appears to be a much better approximation for $P(\log \epsilon_0)$ than for $P(\log \chi_0)$ should be predicated on the existence (or not) of an inertial subrange. For why this may be so, we refer to the discussion in Mi et al. [9] of the implications on $P(\log \chi_0)$ of the statistical interdependence of ϕ and χ_0. The results in §III B and §IV B indicate the existence of a well-developed inertial range in the current simulations.

We compute $P(\log \epsilon_0)$ and $P(\log \chi_0)$ in terms of histograms with variable width bins such that there are the same number of samples in each bin. This method may not be ideal if the extreme tails of the distributions are of interest. However, it enables an estimate to be made of the statistical uncertainly by plotting the probability densities at the locations of the mean of the samples in each bin, with a horizontal error bar with length equal to the standard deviation in the bin. Each bin includes 67 million samples for cases ϕ_b, ϕ_c, and ϕ_d, and 203 million samples for case ϕ_a. The PDFs are plotted in figure 9. Also plotted is the standard Gaussian.

It is evident from the figure that the Gaussian is an excellent model for $P(\log \epsilon_0)$ for many purposes, particular for large values of $\log \epsilon_0$. For low values, the PDF lies outside the Gaussian, but the details are beyond the scope of this paper. Of interest is the shape of $P(\log \chi_0)$ compared with that of $P(\log \epsilon_0)$. For the cases with $\mathrm{Sc} \leq 1$, the PDFs of $\log \chi_0$ are the same to within the error bars, and their righthand tails are distinctly lower than than that of $\log \epsilon_0$. This is consistent with the literature cited earlier in this section. The PDF for $\mathrm{Sc} = 7$, however, is markedly different from the others and much closer to that of $\log \epsilon_0$. It is still not as close to the Gaussian model as $P(\log \epsilon_0)$, and we again refer to the discussion in Mi et al. [9] as to whether $P(\log \chi_0)$ can, in theory, be Gaussian. Nevertheless, the insensitivity of $P(\log \chi_0)$ to Sc for $Sc \in [0.01, 1]$, and the strong difference in $P(\log \chi_0)$ between $\mathrm{Sc} = 1$ and $\mathrm{Sc} = 7$ is interesting. One explanation is that when there is sufficient scale separation between η_k and η_b, then larger values of χ_0 can develop. The modeling implication of this result, taken in conjunction with the PDF characteristics reported by Shete and de Bruyn Kops [48], is that when inertial-convection and viscous-convective subranges exist, then then $P(\log \epsilon_0)$ and $P(\log \chi_0)$ can both be well-approximated by the Gaussian model, at least within three or so standard deviations from the mean.

The convergence to Gaussianity of the logarithm of the dissipation rate ϵ_0 was first suggested by Oboukhov [33], who stated that "any essentially positive characteristic can be represented by a logarithmically Gaussian distribution with correct values of the first two moments". As the Reynolds number becomes large, the dissipation rate ϵ_0 becomes

more intermittent, with more scale separation between samples, and the samples of ϵ_0 become more independent. Therefore, from the Central Limit Theorem, one would expect that, as the Reynolds number becomes large, the probability distribution of the logarithm of ϵ_0 would approach Gaussian. Similarly, if the Schmidt number also becomes large, then χ_0 also becomes more intermittent, with more scale separation between samples, and the samples of χ_0 become more independent. Therefore the Central Limit Theorem would also suggest that the probability distribution of the logarithm of χ_0 would approach Gaussian. Provided that Re_λ is large, as it is in the current simulations, just how large Sc need be is indicated in figure 9.

V. DISCUSSION AND CONCLUSIONS

Our motivation for this research is the classical notion that the statistics of a passive scalar can be expected to be similar to the analogous velocity statistics given sufficiently high Reynolds number. The thought is that if there is sufficient scale separation between the flow-specific large-scale structures and some smaller length scales of interest, then the statistics of those smaller scales will follow those of velocity. Our cited review points out that there are theoretical reasons why the velocity and scalar statistics cannot be the same. Nevertheless, the large number of studies on the effect of Reynolds and Schmidt number on scalar statistics suggests that many researchers expect that, given sufficient scale separation, the scalar statistics will follow the velocity statistics, at least sufficiently well for many modeling applications.

The reviewed literature indicated that results are limited either by dynamic range, in the case of laboratory and numerical experiments, or by measurement limitations, in the case of in-situ measurements of the ocean and atmosphere. As a consequence, there are no detailed measurements of both the velocity and scalar statistics at high Reynolds number and high Schmidt number. Therefore, while scale separation has been considered in terms of high Reynolds number or high Schmidt number, we know of no detailed studies in which both were simultaneously high and detailed velocity and scalar statistics were measured. This leads to our hypothesis that two types of scale separation are required for the scalar statistics to approach those of velocity. First, there must be an inertial-convective subrange so that the velocity statistics can be approximately universal. Given this, there must also be an viscous-convective range so that the scalar has the opportunity to adjust to the smallest turbulent velocity motions without such adjustment being precluded by diffusive effects.

To test this hypothesis for mixing of heat in air and water, we develop a DNS data set of homogeneous isotropic turbulence that has a clear inertial range with $\mathrm{Re}_\lambda = 633$. Based on recently published resolution criteria [47, 48], we conclude that our simulations are sufficiently resolved for accurately computing small-scale statistics. By considering scalars with and without a viscous-convective range, we observe the effect of high Sc, given high Re_λ. Importantly, the simulations are in broad agreement with the similarity theories of KOCB.

An assumption in all the classical similarity hypotheses is that there exists a range of length scales at which the scalar statistics are isotropic. If the scalar is isotropic, then the skewness of the scalar derivatives will be zero. Due to the ramp-cliff structures that form in the scalar field, the skewness is not zero, but it has been shown elsewhere to scale with $\mathrm{Sc}^{-1/2}$ provided $\mathrm{Sc} \geq 1$, and to be independent of Re_λ. Our data affirm this conclusion. This scaling argument supports our hypothesis because it does not hold for $\mathrm{Sc} < 1$. That is, scale separation associated with high Reynolds number alone does not result in small scales of the scalar approaching isotropy; however, scale separation associated with both high Schmidt and Reynolds numbers does, in which case the $Sc^{-1/2}$ scaling is observed for skewness.

Next we turn to the intermittency exponents for the scalar and velocity. The exponent for velocity is widely thought to be at least approximately universal with $\mu = 0.25 \pm 0.05$, and our data are consistent with this. Consistent with the literature, the exponent for the scalar is significantly larger than μ except, importantly, for the case of $\mathrm{Sc} = 7$, for which the two exponents are very nearly the same. This result supports our conjecture that scale separation between the smallest turbulent velocity fluctuations and the smallest scalar fluctuations is required for the velocity and scalar statistics to be similar, at least in the range of Schmidt numbers considered. Given that the intermittency exponents are defined in the inertial subrange, high Re_λ is a necessary condition for evaluating μ and μ_ϕ.

More broadly, internal intermittency is characterized by the breadth of the PDFs of ϵ_0 and χ_0. It has long been an open question why the lognormal model is fairly good for the ϵ_0, except for the most extreme values, but not a good model for even moderately high values of χ_0. The DNS data show that $P(\log \chi_0)$ is insensitive to Sc for $\mathrm{Sc} \leq 1$, but differs markedly between $\mathrm{Sc} = 1$ and $\mathrm{Sc} = 7$. Not only is the PDF very sensitive to the existence of a viscous-convective subrange, the lognormal model is fairly good for χ_0 when $\mathrm{Sc} = 7$. It is not as good as it is for ϵ_0, but the results suggest that it might be a much more practical model for mixing in water than in air.

The observation that the scalar derivative skewness, intermittency exponent, and PDF shape all approach the analogous statistics for velocity provided $\mathrm{Sc} > 1$ but not when $\mathrm{Sc} \leq 1$ suggests that the existence of a viscous-convective subrange is essential to effectively apply the attractive but unproven idea that scalar modeling can be expected to be simpler given sufficient scale separation. An inertial-convective subrange is prerequisite to apply similarity theories

extending from the work of KOBC to model scalars, but it is not sufficient. It appears that the existence of both inertial-convective and viscous-convective ranges are required for the velocity field to be approximately universal and for the scalar statistics to adjust to those of velocity field.

ACKNOWLEDGEMENTS

High performance computing resources were provided through the U.S. Department of Defense High Performance Computing Modernization Program by the Army Engineer Research and Development Center. This research was supported by the Office of Naval Research via grants N00014-12-1-0583, N00014-19-1-2152, and N00014-19-1-2154.

Appendix A: The skewness model given in equation (10) and implicit assumptions

We are not aware of a published derivation of (10) and so provide one, following some of the statements in Sreenivasan [59]. We provide this to make the assumptions in the derivation to be more explicit. Let δ be the scale of the cliff, and L be the scale of the ramp. We start with what's given in Sreenivasan [59, Page 5 and figure 5],

$$\langle (d\phi/dz)^p \rangle \sim \left(\frac{\Delta\phi}{\delta}\right)^p \times \frac{\delta}{L} \tag{A1}$$

where $\Delta\phi$ is the maximum change in ϕ that corresponds to the height of the cliff and p is a positive odd integer. Since ϕ is gaussian-like, $\Delta\phi \sim \phi_{rms}$. Therefore,

$$\langle (d\phi/dz)^p \rangle \sim \left(\frac{\phi_{rms}}{\delta}\right)^p \times \frac{\delta}{L}. \tag{A2}$$

This forms the numerator of (10). For even ordered moments, isotropy and the scalar dissipation anomaly give

$$\langle (d\phi/dz)^2 \rangle \sim \frac{1}{3D}\chi \sim \frac{1}{3D}\frac{\phi_{rms}^2 u'}{L}. \tag{A3}$$

where u' is the rms velocity fluctuation. As mentioned in §IV A, this relation should be considered an approximation. Dividing (A2) by (A3) raised to $p/2$, we get

$$\frac{\langle (d\phi/dz)^p \rangle}{\langle (d\phi/dz)^2 \rangle^{p/2}} \sim \frac{(\phi_{rms}/\delta)^p \times (\delta/L)}{(\phi_{rms}^2 \frac{u'}{LD})^{p/2}}. \tag{A4}$$

For $Sc > 1$, $\delta = \eta_b = \eta_k Sc^{-1/2}$. Also, standard scaling relations $\frac{L}{\eta_k} \sim {\rm Re}_\lambda{}^{3/2}$ and ${\rm Re}_\lambda{}^2 \sim Re \sim \frac{u'L}{\nu}$ are used. Substituting in (A4) and cancelling terms, we get

$$\frac{\langle (d\phi/dz)^p \rangle}{\langle (d\phi/dz)^2 \rangle^{p/2}} \sim Sc^{-1/2}{\rm Re}_\lambda{}^{-3/2}\frac{(1/\delta)^p}{(\frac{u'}{LD})^{p/2}} = Sc^{-1/2}{\rm Re}_\lambda{}^{-3/2}\left(\frac{1}{\delta^2}\frac{LD}{u'}\right)^{p/2} \tag{A5}$$

$$= Sc^{-1/2}{\rm Re}_\lambda{}^{-3/2}\left(\frac{Sc}{\eta_k^2}\frac{LD}{u'}\right)^{p/2} \tag{A6}$$

$$= Sc^{-1/2}{\rm Re}_\lambda{}^{-3/2}\left(\frac{Sc}{\eta_k^2}\frac{L^2 D}{\nu {\rm Re}_\lambda{}^2}\right)^{p/2} \tag{A7}$$

$$= Sc^{-1/2}{\rm Re}_\lambda{}^{-3/2}\left(\frac{L^2}{\eta_k^2}\frac{1}{{\rm Re}_\lambda{}^2}\right)^{p/2} \tag{A8}$$

$$= Sc^{-1/2}{\rm Re}_\lambda{}^{-3/2}\left({\rm Re}_\lambda{}^{3/2}\frac{1}{{\rm Re}_\lambda}\right)^{p} \tag{A9}$$

$$= Sc^{-1/2}{\rm Re}_\lambda{}^{(p-3)/2} \tag{A10}$$

which is (10).

Let us consider the implicit assumptions in this derivation. A required result for the above justification is the scalar dissipation anomaly given in (A3), the conditions for the validity of which have been described in Donzis et al. [74]. They propose an model form for χ as

$$\frac{\langle \phi^2 \rangle}{\chi\, T} = c_1 \left(f_1^{2/3} - \frac{c3}{\mathrm{Re}_\lambda} \right) + c_2 \frac{ln(Sc)}{\mathrm{Re}_\lambda} \tag{A11}$$

where f_1 is given as

$$f_1 = A(1 + \sqrt{1 + (B/\mathrm{Re}_\lambda)^2}). \tag{A12}$$

This indicates that high Re_λ is an independent requirement to achieve asymptotic values of χ. In particular, they mention clearly in Donzis et al. [74, eq. 3.8, eq. 3.10] that for χ to asymptote to a value (to be independent of Sc), the Re_λ needs to be independently high, for both $Sc > 1$ and $Sc < 1$. The values of required Re_λ for the asymptotic state to occur have been proposed to be $\mathrm{Re}_\lambda > 200$ for $1 \leq Sc \leq 10$, limits for other values of Sc can be seen in Donzis et al. [74, figure 11].

Thus, the derivation of (10) assumes both high $\mathrm{Re}_\lambda$and high Sc or, in other words, the existence of both the intertial convective and viscous-convective subranges. This explains the behavior observed in figure 7.

[1] A. M. Oboukhov. Structure of temperature field in a turbulent flow. *Izv. Akad. Nauk. SSSR, Geogr. i Geofiz*, 13:58–69, 1949.

[2] S. Corrsin. On the spectrum of isotropic temperature fluctuations in an isotropic turbulence. *J. Appl. Phys.*, 22:469–472, 1951.

[3] G. K. Batchelor. Small-scale variation of convected quantities like temperature in turbulent fluid. Part 1. general discussion and the case of small conductivity. *J. Fluid Mech.*, 5:113, 1959.

[4] G. K. Batchelor, I. D. Howells, and A. A. Townsend. Small-scale variation of convected quantities like temperature in turbulent fluid. Part 2. the case of large conductivity. *J. Fluid Mech.*, 5(1):134–139, 1959.

[5] A. N. Kolmogorov. Local structure of turbulence in an incompressible fluid at very high Reynolds numbers. *Dokl. Akad. Nauk SSSR*, 30:299–303, 1941.

[6] A. M. Oboukhov. Spectral energy distribution in a turbulent flow. *Dokl. Akad. Nauk. SSSR*, 32:22–24, 1941a.

[7] A. M. Oboukhov. Spectral energy distribution in a turbulent flow. *Izv. Akad. Nauk. SSSR, Ser. Geogr. i. Geofiz*, 5:453–466, 1941b.

[8] K. R. Sreenivasan. On local isotropy of passive scalars in turbulent shear flows. *Proc. R. Soc. Lond. A*, 434(1890):165–182, 1991.

[9] J. Mi, R.A. Antonia, G.J. Nathan, and R.E. Luxton. Non-gaussian statistics of a passive scalar in turbulent flows. In *Symposium (International) on Combustion*, volume 27, pages 989–995. Elsevier, 1998.

[10] Z. Warhaft. Passive scalar in turbulent flows. *Annu. Rev. Fluid Mech.*, 32:203–240, 2000.

[11] R. J. Hill. Models of the scalar spectrum for turbulent advection. *J. Fluid Mech.*, 88(3):541–562, 1978.

[12] J. E. Paquin and S. Pond. The determination of the kolmogoroff constants for velocity, temperature and humidity fluctuations from second-and third-order structure functions. *J. Fluid Mech.*, 50(2):257–269, 1971.

[13] C. H. Gibson and W. H. Schwarz. The universal equilibrium spectra of turbulent velocity and scalar fields. *J. Fluid Mech.*, 16:365, 1963.

[14] H. L. Grant, B. A. Hughes, W. M. Vogel, and A. Moilliet. The spectrum of temperature fluctuations in turbulent flow. *J. Fluid Mech.*, 34(3):423–442, 1968.

[15] S.-C. Lin and S.-C. Lin. Study of strong temperature mixing in subsonic grid turbulence. *Phys. Fluids*, 16(10):1587–1598, 1973.

[16] R. M. Williams and C. A. Paulson. Microscale temperature and velocity spectra in the atmospheric boundary layer. *J. Fluid Mech.*, 83(3):547–567, 1977.

[17] F. H. Champagne, C. A. Friehe, J. C. LaRue, and J. C. Wynagaard. Flux measurements, flux estimation techniques, and fine-scale turbulence measurements in the unstable surface layer over land. *J. Atmost. Sci.*, 34(3):515–530, 1977.

[18] N. E. J. Boston and R. W. Burling. An investigation of high-wavenumber temperature and velocity spectra in air. *J. Fluid Mech.*, 55(3):473–492, 1972.

[19] C. H. Gibson, Stegen G. R., and Williams R. W. Statistics of the fine structure of turbulent velocity and temperature fields measured at high Reynolds number. *J. Fluid Mech.*, 41:153–167, 1970.

[20] J.P. Clay. *Turbulent mixing of temperature in water, air and mercury.* PhD thesis, University of California at San Diego, 1973.

[21] J. Qian. Variational approach to the closure problem of turbulence theory. *Phys. Fluids*, 26(8):2098–2104, 1983.

[22] J. Qian. Universal equilibrium range of turbulence. *Phys. Fluids*, 27(9):2229–2233, 1984.

[23] J. Qian. A passive scalar field convected by turbulence. *Phys. Fluids*, 28(5):1299–1304, 1985.

[24] T. Watanabe and T. Gotoh. Statistics of a passive scalar in homogeneous turbulence. *New J. Phys.*, 6(40):1–36, 2004.

[25] R. A. Antonia and P. Orlandi. On Batchelor constant in decaying isotropic turbulence. *Phys. of Fluids*, 15(7):2084–2086, 2003.

[26] R. O. Fox. *Computational Models for Turbulent Reacting Flows*, pages 274–275. Cambridge University Press, Cambridge, UK, 2003.

[27] P. E. Dimotakis. Turbulent mixing. *Annu. Rev. Fluid Mech.*, 37:329–356, 2005.

[28] W. Heisenberg. Zur statistischen theorie der turbulenz. *Z. Phys.*, 124:628–657, 1948.

[29] S. B. Pope. *Turbulent Flows*. Cambridge University Press, Cambridge, 2000.

[30] J. Meyers and C. Meneveau. A functional form for the energy spectrum parametrizing bottleneck and intermittency effects. *Phys. Fluids*, 20(0):065109, 2008.

[31] A. Muschinski and S. M. de Bruyn Kops. Investigation of Hill's optical turbulence model by means of direct numerical simulation. *J. Opt. Soc. Am. A*, 32(12):2423–2430, 2015.

[32] A. N. Kolmogorov. A refinement of previous hypotheses concerning the local structure of turbulence in a viscous incompressible fluid at high Reynolds number. *J. Fluid Mech.*, 13:82–85, 1962.

[33] A. M. Oboukhov. Some specific features of atmospheric turbulence. *J. Fluid Mech.*, 13:77–81, 1962.

[34] E. A. Novikov and R. W. Stewart. The intermittency of turbulence and the spectrum of energy dissipation. *Izv., Akad. Nauk. SSSR, Ser. Geoffiz*, 3:408–413, 1964.

[35] T. Zhou and R. A. Antonia. Approximations for turbulent energy and temperature variance dissipation rates in grid turbulence. *Phys. Fluids*, 12(2):335–344, 2000.

[36] P. K. Yeung, D. A. Donzis, and K. R. Sreenivasan. High-Reynolds-number simulation of turbulent mixing. *Phys. Fluids*, 17:081703, 2005.

[37] T. Ishihara, Y. Kaneda, M. Yokokawa, K. Itakura, and A. Uno. Small-scale statistics in high-resolution direct numerical simulation of turbulence: Reynolds number dependence of one-point velocity gradient statistics. *J. Fluid Mech.*, 592: 335–366, 2007.

[38] T. Ishihara, K. Morishita, M. Yokokawa, A. Uno, and Y. Kaneda. Energy spectrum in high-resolution direct numerical simulations of turbulence. *Phys. Rev. Fluids*, 1:082403, Dec 2016.

[39] S. A. Orszag and G. S. Patterson. Numerical simulation of turbulence. In M. Rosenblatt and C. Van Atta, editors, *Statistical Models and Turbulence*, volume 12 of *Lecture Notes in Physics*, pages 127–147. Springer, New York, 1972.

[40] J. J. Riley, R. W. Metcalfe, and M. A. Weissman. Direct numerical simulations of homogeneous turbulence in density stratified flows. In B. J. West, editor, *Proc. AIP Conf. Nonlinear Properties of Internal Waves*, pages 79–112. American Institute of Physics, New York, 1981.

[41] J. Kim, P. Moin, and R. D. Moser. Turbulence statistics in fully developed channel flow. *J. Fluid Mech.*, 177:133–166, 1987.

[42] M. M. Rogers and R. D. Moser. Direct simulation of a self-similar turbulent mixing layer. *Phys. Fluids*, 6:903–923, 1994.

[43] S. M. de Bruyn Kops and J. J. Riley. Direct numerical simulation of laboratory experiments in isotropic turbulence. *Phys. Fluids*, 10(9):2125–2127, 1998.

[44] S. M. de Bruyn Kops and J. J. Riley. Re-examining the thermal mixing layer with numerical simulations. *Phys. Fluids*, 12(1):185–192, 2000.

[45] D. Gottlieb and S. A. Orszag. *Numerical Analysis of Spectral Methods: Theory and Applications*, volume 26 of *NSF-CBMS, Regional Conference Series in Applied Mathematics*. Society of Industrial and Applied Mathematics, Philadelphia, 1977.

[46] V. Eswaran and S. B. Pope. Direct numerical simulations of the turbulent mixing of a passive scalar. *Phys. Fluids*, 31: 506–520, 1988.

[47] P. K. Yeung, K. R. Sreenivasan, and S. B. Pope. Effects of finite spatial and temporal resolution in direct numerical simulations of incompressible isotropic turbulence. *Phys. Rev. Fluids*, 3(6):064603, 2018.

[48] K.P. Shete and S.M. de Bruyn Kops. Area of scalar isosurfaces in homogeneous isotropic turbulence as a function of reynolds and schmidt numbers. *J. Fluid Mech.*, 2019.

[49] J. B. Perot and S. M. de Bruyn Kops. Modeling turbulent dissipation at low and moderate Reynolds numbers. *J. Turbulence*, 7:1–14, 2006.

[50] K. R. Sreenivasan. An update on the energy dissipation rate in isotropic turbulence. *Phys. Fluids*, 10(2):528–529, 1998.

[51] M. R. Overholt and S. B. Pope. A deterministic forcing scheme for direct numerical simulations of turbulence. *Comput. Fluids*, 27:11–28, 1998.

[52] K. J. Rao and S. M. de Bruyn Kops. A mathematical framework for forcing turbulence applied to horizontally homogeneous stratified flow. *Phys. Fluids*, 23:065110, 2011. doi:doi:10.1063/1.3599704.

[53] S. Almalkie and S. M. de Bruyn Kops. Energy dissipation rate surrogates in incompressible Navier-Stokes turbulence. *J. Fluid Mech.*, 697:204–236, 2012.

[54] D. A. Donzis and K. R. Sreenivasan. The bottleneck effect and the Kolmogorov constant in isotropic turbulence. *J. Fluid Mech.*, 657:171–188, 2010.

[55] R. H. Kraichnan. Small-scale structure of a scalar field convected by turbulence. *Phys. Fluids*, 11:945–963, 1968.

[56] P. G. Mestayer, C. H. Gibson, M. F. Coantic, and A. S. Patel. Local anisotropy in heated and cooled turbulent boundary layers. *Phys. Fluids*, 19(9):1279–1287, 1976.

[57] K. R. Sreenivasan and R. A. Antonia. Skewness of temperature derivatives in turbulent shear flows. *Phys. Fluids*, 20(12): 1986–1988, 1977.

[58] B. I. Shraiman and E. D. Siggia. Scalar turbulence. *NATURE*, 405(8):639–646, 2000.

[59] K. R. Sreenivasan. Turbulent mixing: a perspective. *Proceedings of the National Academy of Sciences*, 2018:201800463, 2018. ISSN 0027-8424. doi:10.1073/pnas.1800463115.

[60] Dhawal Buaria, Matthew P Clay, Katepalli R Sreenivasan, and PK Yeung. Turbulence is an ineffective mixer when schmidt numbers are large. *Physical Review Letters*, 126(7):074501, 2021.
[61] C. W. Van Atta. Influence of fluctuations in local dissipation rates on turbulent scalar characteristics in the inertial subrange. *Phys. of Fluids*, 14:1803–1804, 1971.
[62] J. L. W. V. Jensen. Sur les fonctions convexes et les inégalités entre les valeurs moyennes. *Acta Mathematica*, 30(1): 175–193, 1906.
[63] A. Praskovsky and S. Oncley. Comprehensive measurements of the intermittency exponent in high Reynolds number turbulent flows. *Fluid Dyn. Res.*, 21(5):331–358, 1997.
[64] K. R. Sreenivasan and R. A. Antonia. The phenomenology of small-scale turbulence. *Annu. Rev. Fluid Mech.*, 29:435–472, 1997.
[65] L. Mydlarski and Z. Warhaft. Passive scalar statistics in high Péclet number grid turbulence. *J. Fluid Mech.*, 358:135–175, 1998.
[66] A. Muschinski. Local and global statistics of clear-air Doppler radar signals. *Radio Sci.*, 39:RS1008, 2004.
[67] R. Prasad, C. Meneveau, and K. R. Sreenivasan. The multifractal nature of the dissipation of passive scalars in fully turbulent flows. *Phys. Rev. Lett.*, 61:74–77, 1988.
[68] S. M. de Bruyn Kops. Classical turbulence scaling and intermittency in stably stratified Boussinesq turbulence. *J. Fluid Mech.*, 775:436–463, 2015.
[69] R. S. Miller, F. A. Jaberi, C. K. Madnia, and P. Givi. The structure of the small-scale intermittency of passive scalars in homogeneous turbulence. *Journal of Scientific Computing*, 10(1):151–180, 1995.
[70] C. N. Markides and E. Mastorakos. Measurements of the statistical distribution of the scalar dissipation rate in turbulent axisymmetric plumes. *Flow, Turbulence and Combustion*, 81(1-2):221–234, 2008.
[71] R. A. Antonia and K. R. Sreenivasan. Lognormality of temperature dissipation in a turbulent boundary layer. *Phys. Fluids*, 20(11):1800–1804, 1977.
[72] Alain Pumir, Boris I Shraiman, and Eric D Siggia. Exponential tails and random advection. *Physical review letters*, 66 (23):2984, 1991.
[73] P. Vedula, P. K. Yeung, and R. O. Fox. Dynamics of scalar dissipation in isotropic turbulence: a numerical and modelling study. *J. Fluid Mech.*, 433:29–60, 2001.
[74] D. A. Donzis, K. R. Sreenivasan, and P. K. Yeung. Scalar dissipation rate and dissipative anomaly in isotropic turbulence. *J. Fluid Mech.*, 532:199–216, 2005.